J Fusion Energ
DOI 10.1007/s10894-011-9414-3

ORIGINAL RESEARCH

Model Parameters Versus Gas Pressure in Two Different Plasma Focus Devices Operated in Argon and Neon

Sh. Al-Hawat · M. Akel · S. Lee · S. H. Saw

Abstract For the plasma focus device AECS PF-2 operated in Ar and INTI PF in Ne, model parameters of mass and current in the axial phase of plasma focus were found by matching the measured and calculated current waveforms over a range of pressures. The results show a value of $f_m = 0.05 \pm 0.01$ over 0.2–1.2 Torr in Ar; and $f_m = 0.04 \pm 0.01$ over 0.7–4.1 Torr in Neon. The value of $f_c = 0.7$ was fitted for all cases. Combining these results with those published for several other small machines it would appear that, where measured current waveforms are not available for example in designing new machines, a good compromise would be to take a guideline value of $f_m = 0.05$ and $f_c = 0.7$ for both Argon and Neon.

Keywords Lee model · Model parameters · Plasma focus device · Argon · Neon

Sh. Al-Hawat (✉) · M. Akel
Department of Physics, Atomic Energy Commission, P.O. Box 6091, Damascus, Syria
e-mail: scientific@aec.org.sy

S. Lee · S. H. Saw
Institute for Plasma Focus Studies, 32 Oakpark Drive, Chadstone VIC 3148, Australia

S. Lee · S. H. Saw
INTI International University, 71800 Nilai, Malaysia

S. Lee
National Institute of Education, Nanyang Technological University, Singapore 637616, Singapore

Introduction

The plasma focus radiative model—Lee Model has been developed for Mather-type plasma focus devices like UNU/ICTP PFF [1, 2]. But in principle, there is no limit to energy storage and electrode configuration, so it could be used for any plasma focus device. The model has been used for applications such as design optimization of plasma focus devices [3], to estimate the soft x-ray production [4–6] and neutron yields [7] and to find the focus pinch current waveform from a measured discharge current waveform [8].

The equation of motion and the circuit (current) equation for the axial phase include model parameters f_m and f_c, where f_m is the fraction of mass swept down the tube in the axial direction of the current sheath, f_c is the fraction of current flowing in the magnetic piston.

The model equations for the radial phase include parameters f_{mr} and f_{cr} where f_{mr} describes the effective mass swept into the radial slug. It is found that f_{mr} is typically larger than f_m of the axial phase and that f_{cr} is almost the same as the f_c in the axial phase [9, 10].

In this work, we carry out measurements of current waveforms versus pressure for Ar and Ne to find the axial phase model parameters f_m, f_c versus the filling gas pressure on two different PF devices: AECS PF-2 in filling gas of Ar and INTI PF in filling gas of Ne. We also compare our results, with experimental results of published data taken from several other machines [4, 11, 12].

Experimental Set Up

The experimental set-up with the equivalent circuit for both two devices used in this study are shown in Fig. 1a, b, respectively.

Published online: 22 April 2011

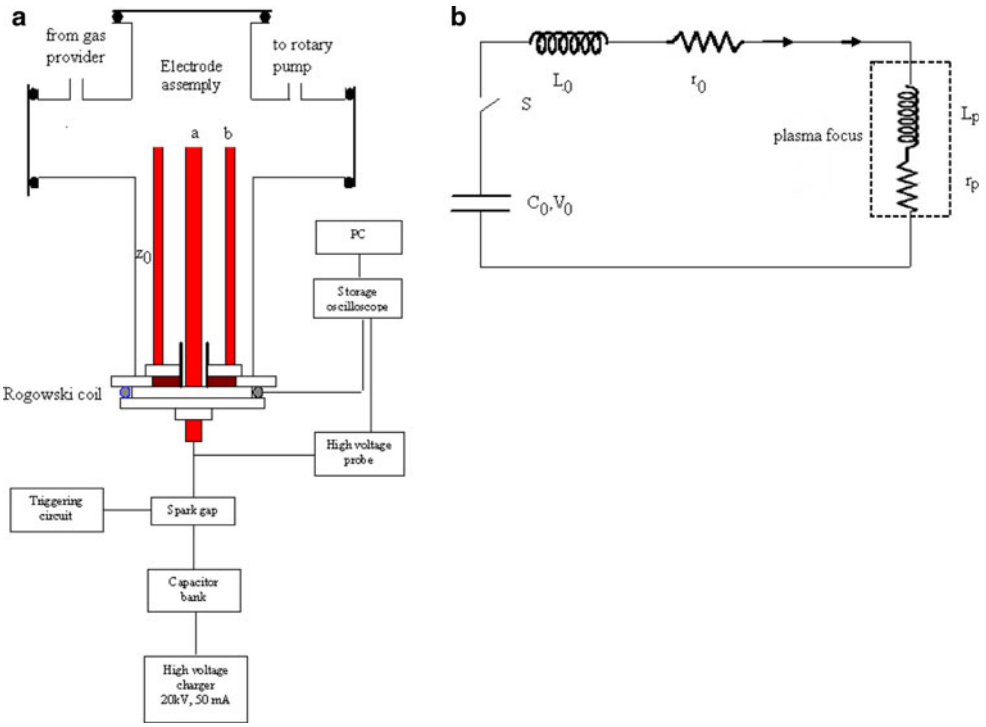

Fig. 1 **a** Experimental set up for AECS PF-2 and INTI PF devices. The main parts of those systems are as shown on the schematic diagram; where z_0 is the anode length, a is the anode radius, b is the radius of the cathode position. **b** Equivalent electrical circuit of the plasma focus device; where L_0, C_0, r_o are inductance, capacitance and resistance of the external circuit respectively; L_p and r_p are inductance and resistance of the plasma focus

The experimental setup as shown in Fig. 1a, consists of: a plasma focus tube; charger; storage capacitor bank; spark gap; triggering unit; storage oscilloscope; PC computer; voltage divider; and Rogowski coil; whereas the equivalent circuit indicates the external part with C_0, L_0, r_0 and the internal part with L_p and r_p for plasma.

The plasma focus chamber is made of stainless steel; it is 30 cm long and 16 cm in diameter. The central electrode is made of copper rod 16 cm long and 1.9 cm in diameter; it forms the anode of the focus tube. The cathode of the focus consists of six copper rods which are placed symmetrically around the anode at a radial distance of 3.2 cm, the diameter of each rod is 8 mm and its length is of 16 cm. To establish current sheath with axial symmetry the anode bottom was surrounded by a Pyrex glass tube as a back-wall.

So, the energy, tube, bank and operating parameters are:

For AECS PF-2: $E = 2.8$ kJ, $c = b/a = 3.4$, $a = 0.95$ cm, $b = 3.2$ cm, $z_0 = 16$ cm, $L_0 = 270$ nH, $C_0 = 25$ μF, $r_0 = 35$ mΩ and $V_0 = 15$ kV.
And for INTI PF: $E = 2.2$ kJ, $c = b/a = 3.4$, $a = 0.95$ cm, $b = 3.2$ cm, $z_0 = 16$ cm, $L_0 = 110$ nH, $C_0 = 30$ μF, $r_0 = 12$ mΩ and $V_0 = 12$ kV.

where E is the storage energy of capacitor bank; 'a' is the anode radius; 'b' is the cathode radius; z_0 is the anode length; L_0 is the external inductance; C_0 is the capacitance of the bank capacitors; r_0 is the stray resistance.

The experiments were carried out on both devices; the first one in the filling gas of Ar with varying pressure in between 0.12 and 1.2 Torr; and the second one in the filling gas of Ne with varying pressure in between 0.7 and 4.1 Torr.

From the current waveform shown in Fig. 2, which represents the temporal evolution of the current at 5 mbar in Ar, we can find the period of current oscillations $T = 17.35$ μs. Following the calibration method of Rogowski coil described in [13] we found that the calibration coefficient was 2.6 kA/V for AECS PF-2 taking into account that the current trace shown in Fig. 3a, b was obtained with attenuation of 1:10.

Fitting Procedures

In this work, we are going to fit the computed and measured current varying the pressure, with the purpose to find the proper model parameters versus pressure for both devices and filling gases (Ar & Ne).

To do that, the code RADPF5.15d of Lee model written in Visual Basic and supported by Excel window was used with data from experiments carried out on AECS PF-2 and INTI PF. To run the code, we use the following bank, tube and operating parameters: for AECS PF-2 device:

Bank parameters: $L_0 = 270$ nH, $C_0 = 25$ μF, $r_0 = 35$ mΩ
Tube parameters: $z_0 = 16$ cm, $a = 0.95$ cm, $b = 3.2$ cm;
Operation parameters: $V_0 = 15$ kV, $p_0 = 0.12$-1.2 Torr, MW = 40, A = 18, At-Mol = 1 (for Ar)

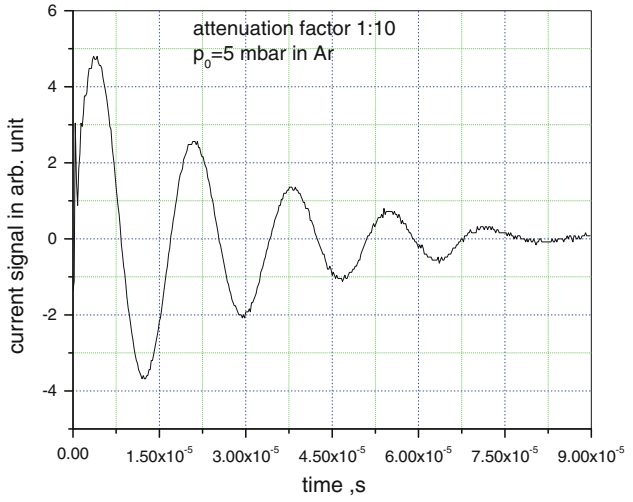

Fig. 2 The temporal evolution of the current waveform for AECS PF-2 at 5 mbar in Ar

And the following for INTI PF device:

Bank parameters: $L_0 = 110$ nH, $C_0 = 30$ μF, $r_0 = 12$ mΩ;
Tube parameters: $z_0 = 16$ cm, $a = 0.95$ cm, $b = 3.2$ cm;
Operation parameters: $V_0 = 12$ kV, $p_0 = 0.7$-4.1 Torr, MW = 20, A = 10, At-Mol = 1 (for Ne)

Initially, for fitting the computed current trace to the measured current trace, we do not know the model parameters. We use the trial model parameters recommended in the code as $f_m = 0.073$, $f_c = 0.7$, $f_{mr} = 0.26$, $f_{cr} = 0.7$. For that, we configure the code for AECS PF-2 and INTI PF devices in Ar and Ne respectively; we run the code, and we compare the computed current waveform with the corresponding measured waveform.

The fitting of the axial phase is the first step. This involves variations of f_m and f_c whilst observing the changes that appear on the resulting computed total current trace in respect to the rise time, rising shape and I_{peak}; and how these features compare with the corresponding features of the measured I_{total} trace (see Fig. 3a, b). During this fitting, the increase in f_c increases the axial speed which increases dynamic resistance, thus lowering the current magnitude on the rising slope; this is clearly shown in Fig. 3a, changing the value of f_c from 0.5 to 0.7; whereas a decrease in f_m has almost the same effect also as it is seen from Fig. 3a changing f_m from 0.073 to 0.05.

So, in the fitting process the model parameters are varied in steps starting with f_m and f_c, so that the rising slope leading to the topping profile and peak current and the time of focus are corrected by fitting [9].

Besides f_c and f_m from the model parameters, also the value of stray resistance r_0 needs to be adjusted. We

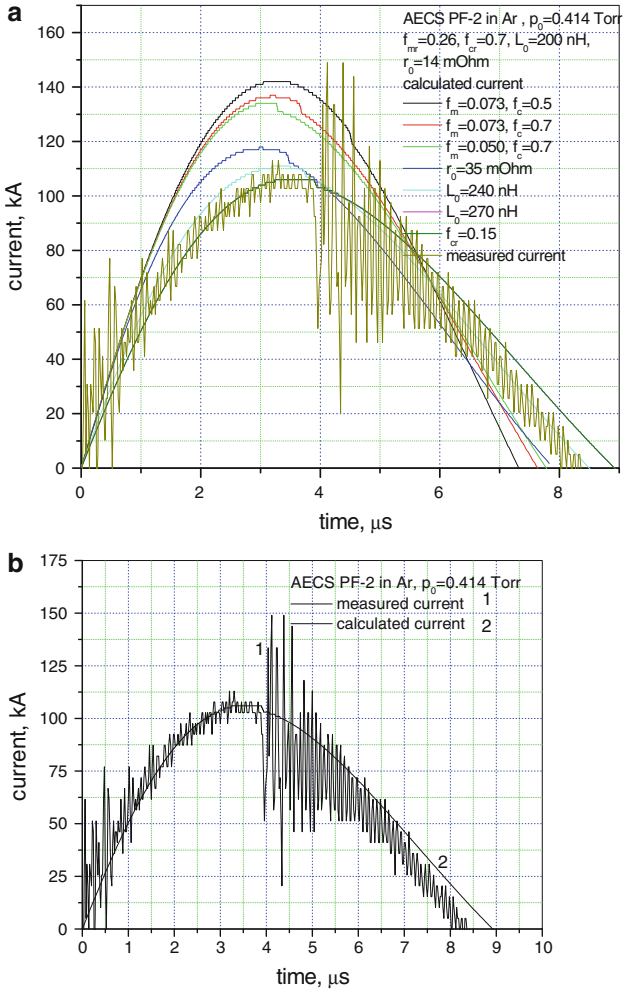

Fig. 3 **a** Current fitting of computed current to measured current traces varying model parameters including external static inductance and stray resistance (L_0, r_0). **b** Current fitting of computed current to measured current traces to obtain fitted parameters $f_m = 0.05$, $f_c = 0.7$, $f_{mr} = 0.15$, $f_{cr} = 0.7$ at $p_0 = 0.414$ Torr

usually start with the small arbitrary value of r_0 as $0.1 \times (L_0/C_0)^{1/2}$; and make needed adjustments as in [10]. In adjusting r_0, we note that an increase of r_0 lowers the current trace at all points proportionately (see Fig. 3a), when r_0 is increased from 14 mΩ to 35 mΩ. In addition to that, sometimes the inductance needs to be adjusted very commonly, the inductance L_0 may be given as the short circuit bank inductance which nominally equals to 200 nH in AECS PF-2. Adjustments to L_0 are indicated, when the computed current rise slope differs significantly from the measured slope. In adjusting L_0 we note that increasing L_0 lowers the slope of the rising current as seen from Fig. 3a moving from $L_0 = 200$–240 nH and in the final step to 270 nH.

Finally, when all values are properly adjusted and when f_m and f_c are correctly fitted, the rising profile of the computed I_{tot}, usually up to the peak value I_{peak} is found to

fit the measured rising profile well in both shape and magnitude.

To fit the whole current trace including the axial and as well as the radial phase, the second step is the fitting of the radial phase. As this phase begins, the current trace starts to roll over, at first imperceptibly, then clearly dipping and then dips sharply as the focus dynamics enters the severe pinch phase which absorbs a significant portion of the energy from the driving magnetic field.

The standard procedure is then to adjust the values of f_{mr} and f_{cr} so that the slope and depth of the current fit the experimentally observed features. However, for the present experiments because the current signals are noisy in the region of the radial phase corresponding to the current dip we have not been able to accurately fit the radial phase model parameters f_{mr} and f_{cr}.

After the previous steps, the fitting has achieved a good agreement in all the features (slopes & magnitudes) of the computed and measured total current traces up to the end of the axial phase and also with approximate fitting for radial phase, as shown, in Fig. 3b.

The exact time profile of the total current trace is governed by the bank parameters (C_0, L_0, r_0) capacitance, external or static inductance, stray resistance, by the focus tube geometry (outer radius of the cathode 'b', inner radius of the anode 'a' and the anode length z_0); and on the operational parameters which are the charging voltage V_0 and the filling pressure p_0 and the nature of the filling gas. It also depends on the fraction of mass swept-up and the fraction of sheath current and the variation of these fractions through the axial and radial phases.

We repeat the previous procedures for a large number of pressures (10 shots for each pressure) ranging between 0.12 and 1.20 Torr in Ar for AECS PF-2 and between 0.7 and 4.1 Torr in Ne for INTI PF; where the average fitting model parameters over shots for each pressure were determined with a maximum absolute error determined as arithmetic error using statistics in Origin software program for each value of pressure and shown in Fig. 4. The fitting procedure is used for all working pressures and the obtained results are shown in Tables 1 and 2 for both devices respectively.

In general, after such fitting for the axial phase and similarly for the radial phase, we will have confidence that the gross features of the studied device including axial and radial trajectories, axial and radial speeds, gross dimensions, densities and plasma temperatures, soft x-ray yields up to the end of radial phase may be well compared with the measured values of the same features.

We emphasis the fact that when the computed total current curve is fitted to the measured curve, we have confidence that the soft X-ray yields are also comparable with what would actually measured.

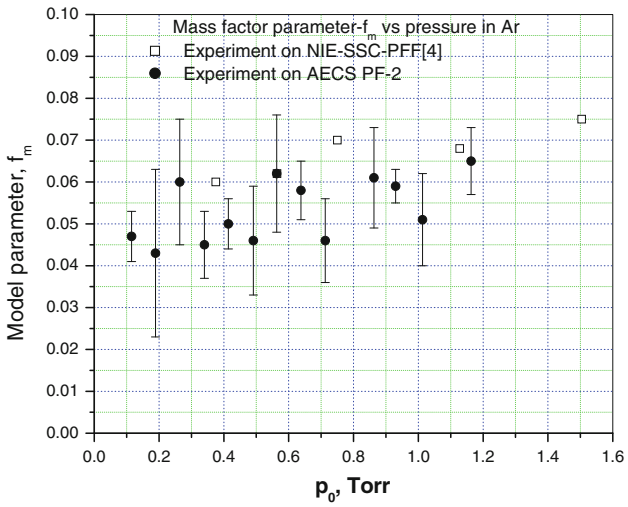

Fig. 4 Comparison of average mass factor f_m values obtained from calculated and measured current waveforms fitting using Lee model code on AECS PF-2 with those measured by magnetic probe on NIE-SSC-PF versus pressure in argon [4]

After finishing the fitting process on AECS PF-2 and INTI PF, we then tabulate the important results of both devices, and do a comparison of model parameters of both devices versus the pressure of Ar and Ne, to obtain important conclusion about their variations.

Results and Discussion

Results are shown in Table 1 and Fig. 4 (for AECS PF-2) and in Table 2 and Fig. 5 (for INTI PF). It was found that the variation of f_m and f_c within each pressure was small enough (±20%), so that their variation with pressure became noticeable although small.

From the fitting results for more than 100 shots, we could quite reasonably interpret the value of f_m to be within the range of 0.05 ± 0.01 over the whole range of pressure 0.2–1.2 Torr in Ar. In other words at one pressure point of operation the value of fitted f_m could vary between the values of 0.04–0.06 (see Fig. 4, the average values range of f_m).

Likewise for the INTI results we would have about the same range of variation of about 0.04 ± 0.01 over the whole range of pressure 0.7-4.1 Torr in neon.

Thus we are able to show that for situations where we do not have a measured current waveform, for argon we may use $f_m = 0.05$ and for neon we may use $f_m = 0.04$. This will facilitate numerical experiments when we are running series of numerical experiments with pressure variation (see Figs. 4, 5).

In Figs. 4 and 5 we also include the results of Tou [11]. Where it was measured f_m of 0.07 for argon in UMDPF1,

Table 1 Calculated results obtained from RADPF 5.15 d of S Lee Model for AECS PF-2 with: E = 2.8 kJ, c = b/a = 3.4, a = 0.95 cm, b = 3.2 cm, z_0 = 16 cm, L_0 = 270 nH, C_0 = 25 μF, r_0 = 35 mΩ, V_0 = 15 kV in argon

p_0, Torr	I_{peak} kA	I_{pinch} start kA	T_{pinch}, min 10^6, K	T_{pinch}, max 10^6, K	Peak v_a cm/μs	Peak v_s cm/μs	Peak v_p cm/μs
0.115	95.3	66.1	16.00	16.14	10.6	49.7	31.2
0.189	100.2	69.4	10.75	10.82	9.3	40.1	27.8
0.264	105.5	72.7	8.45	8.51	7.2	35.6	25.9
0.340	105.3	72.6	6.55	6.73	7.4	30.7	23.1
0.414	106.4	72.7	5.38	5.90	6.5	27.9	21.3
0.491	106.7	72.5	4.5	5.2	6.3	25.5	19.6
0.563	107.9	69.1	3.56	4.47	5.1	22.9	18.0
0.638	105.1	65.2	2.83	3.86	4.8	20.1	15.9
0.713	107.7	69.9	2.91	3.93	5.3	20.4	16.1
0.863	108.9	61.1	2.00	2.76	4.2	16.8	13.3
0.930	109.0	59.9	1.86	2.52	4.0	15.9	12.7
1.013	105.8	57.7	1.69	2.22	4.0	14.8	12.2
1.163	106.5	43.4	1.05	1.23	3.2	10.7	8.2

a_{min} cm	z_{max} cm	Pinch dur, ns	Vmax, kV	N_i pinch, max $(10^{23})/m^3$	Q_{sxr} J	Q_{sxr} %	f_m
0.09	1.3	4.5	27.9	0.208	0	0	0.0470
0.08	1.3	5.3	28.8	0.5	0	0	0.0425
0.07	1.3	5.8	28.7	0.8	0	0	0.060
0.07	1.4	6.8	26.6	1.2	0	0	0.045
0.07	1.4	7.3	24.7	1.5	0	0	0.05
0.06	1.4	7.9	23.0	2.0	0	0	0.05
0.06	1.4	8.7	20.0	2.7	0	0	0.06
0.05	1.4	10.0	25.1	4.9	0	0	0.06
0.04	1.4	9.8	31.5	6.3	0	0	0.05
0.02	1.8	11.8	77.0	45.4	0	0	0.06
0.02	1.8	12.3	65.1	37.7	0	0	0.06
0.02	1.8	13.1	52.6	29.0	0	0	0.05
0.05	1.5	18.7	21.7	7.3	0	0	0.06

f_c	f_{mr}	f_{cr}	EINP %	T axial end μs	SF	ID kA/cm	Qline, J
0.70	0.15	0.70	2.6	2.6	296	100.32	0.003
0.70	0.15	0.70	3.0	2.9	243	105.43	0.018
0.70	0.15	0.70	3.6	3.6	216	111.03	0.057
0.70	0.15	0.70	3.6	3.5	190	110.83	0.163
0.70	0.15	0.70	3.8	3.9	174	111.98	0.337
0.70	0.15	0.70	3.9	4.0	160.2	112.27	0.649
0.70	0.15	0.70	4.0	4.6	151	113.58	1.343
0.70	0.15	0.70	3.9	4.7	139	110.59	2.980
0.70	0.15	0.70	4.1	4.5	134	113	3.885
0.70	0.15	0.70	4.4	5.2	123	115	20.592
0.70	0.15	0.70	4.3	5.3	119	115	21.205
0.70	0.15	0.70	4.0	5.3	111	111	18.805
0.70	0.15	0.70	3.3	2.6	104	112	6.036

Table 1 continued

T radial end μs	Radial duration μs	$\pm\Delta f_m$
2.66	0.06	0.006
2.97	0.06	0.02
3.62	0.07	0.015
3.58	0.08	0.008
3.94	0.08	0.006
4.05	0.09	0.013
4.66	0.10	0.014
4.76	0.11	0.007
4.57	0.12	0.01
5.38	0.15	0.012
5.47	0.15	0.004
5.46	0.16	0.011

Table 2 Calculated results obtained from RADPF 5.15 d of S Lee Model for INTI PF device with: E = 2.2 kJ, c = b/a = 3.4, a = 0.95 cm, b = 3.2 cm, z_0 = 16 cm, L_0 = 110 nH, C_0 = 30 μ*F*, r_0 = 12 mΩ, V_0 = 12 kV in neon

p_0, Torr	I_{peak}, kA	I_{pinch} start, kA	T_{pinch} min, 10^6K	T_{pinch} max, 10^6K	Peak v_a, cm/μs	Peak v_s, cm/μs	Peak v_p, cm/μs
0.7	143.6	97	8.09	9.17	9.2	34.5	24.9
1.0	146.6	98	10.28	11.32	8.7	37.7	27.5
1.5	150.0	95	5.99	6.9	7.4	30.6	21.4
2.0	151.1	93	4.63	5.09	6.9	27.6	18.5
2.5	151.5	92	2.48	2.53	6.7	24.6	15.4
2.9	151.6	92	4.00	4.32	6.7	26.4	17.3
3.5	152.5	89	2.91	3.04	6.3	25	16.1
4.1	153.4	86	2.63	2.71	5.9	24.9	15.7

a_{min}, cm	z_{max}, cm	Pinch dur, ns	V_{max}, kV	N_i pinch max, $10^{23}/m^3$	Q_{sxr}, J	Q_{sxr} %	f_m
0.09	1.4	6.8	27	1.3	0.02	0	0.054
0.09	1.3	6.3	29	1.1	0.01	0	0.045
0.09	1.3	7.6	23	1.8	0.05	0	0.044
0.09	1.3	8.3	21	2.6	0.13	0	0.038
0.08	1.3	7.9	20	7.2	1.11	0.1	0.032
0.09	1.3	8.4	20	3.1	0.21	0	0.028
0.08	1.3	8.3	19	4.9	0.56	0	0.026
0.08	1.2	8.1	18	5.4	0.68	0	0.025

f_c	f_{mr}	f_{cr}	EINP %	T axial end μs	SF	ID, kA/cm	Q_{line}, J
0.7	0.1	0.7	8.9	2.7	181	151	0.02
0.7	0.09	0.7	9.3	2.8	154	154	0.01
0.7	0.1	0.7	9.8	3.2	129	158	0.05
0.7	0.1	0.7	9.9	3.3	112	159	0.13
0.7	0.08	0.7	9.9	3.4	101	160	0.11
0.7	0.08	0.7	9.8	3.4	94	160	0.21
0.7	0.09	0.7	9.9	3.5	86	161	0.56
0.7	0.08	0.7	9.8	3.7	80	161	0.68

Table 2 continued

T radial start, μs	T radial end, μs	Radial dur, μs
2.689	2.754	0.066
2.783	2.842	0.059
3.179	3.255	0.076
3.328	3.415	0.087
3.382	3.497	0.115
3.401	3.494	0.094
3.531	3.638	0.107
3.677	3.789	0.112

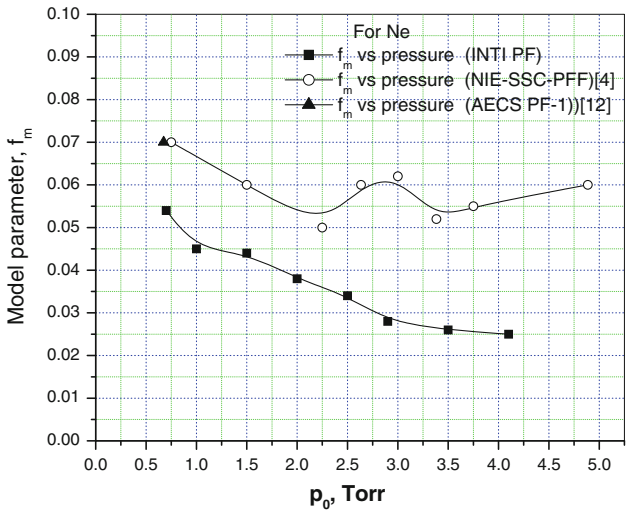

Fig. 5 Comparison mass factor f_m values obtained from calculated and measured current waveforms fitting using Lee model at INTI PF and measured by magnetic probe at NIE-SSC-PF versus pressure in neon [4]

working at 20 kV, 280 kA ignitron-switched plasma focus with $z_o = 16$ cm, $b = 4.3$ cm and $a = 1.3$ cm. In [4] M Liu used magnetic probes to measure f_m, f_c vs pressure in argon and neon on NIE-SSC-PFF, working at 14 kV, 165 kA with $z_o = 16$ cm, $b = 3.2$ cm and $a = 0.95$ cm as provided by Figs. 4 and 5.

So we can conclude that for both devices, the f_m value is small, below 0.1 and generally agrees with the UMDPF1; and that the variation with pressure is not so extensive.

Combining these results with those published for several other small machines (see Figs. 4 and 5) it would appear that, where measured current waveforms are not available for example in designing new machines, a good compromise would be to take a guideline value of $f_m = 0.05$ and $f_c = 0.7$ for both argon and neon.

The obtained results for the main features of plasma focus vs filling gas pressure (peak and pinch currents, pinch temperature, axial, shock and piston speeds, minimum radius and length of pinch, pinch duration, maximum voltage, maximum ion density, X-ray energy, model parameters, percentage of energy input plasma EINP, end axial time, speed factor SF, current per unit length of the anode radius ID, line radiation energy, end radial time, radial duration, and accuracy of f_m) on AECS PF-2 in Ar and on INTI PF in Ne are also tabulated in Tables 1 and 2 respectively.

These tables summarize the results of our numerical experiments using the modified code of Lee model on the data of experiments curried out on AECS PF-2 and INTI PF under certain conditions of pressure, voltage and filling gas.

Coming to the detailed tabulations: we note that the speeds (axial, radial shock and radial piston) and temperature all continue to rise as pressure lowers; similarly speed factor (SF) also increases as pressure is decreased. Pinch length z_{max} is almost a constant. Pinch duration continues to decrease; this is due to better compression at higher speeds. The number density progressively drops, due to the decreasing starting numbers, despite the increasing compression. From Tables 1 and 2, it is noticed that two devices have a different behavior for some features like V_{max} and N_i and Q_{sxr} .

We can also determine without a lot of difficulties the values of the peak current and axial phase duration from the measured and calculated current traces obtained vs the pressure of argon for AECS PF-2 (see Fig. 3a, b for example), as the region of axial phase is less noisy than the radial phase region which starts with the first dip of the strong current oscillations of the current trace. These results are shown in Figs. 6 and 7, respectively. As seen from those, the peak current is slightly increased with pressure; whereas the duration of axial phase is linearly proportioned to the pressure i.e. with the pressure increasing, the current sheath needs more time to reach the top of the anode.

From the calculated results shown in Table 1, it is worthy to notice that soft x-ray line yield of AECS PF-2 in argon is found to be negligible for these operating conditions.

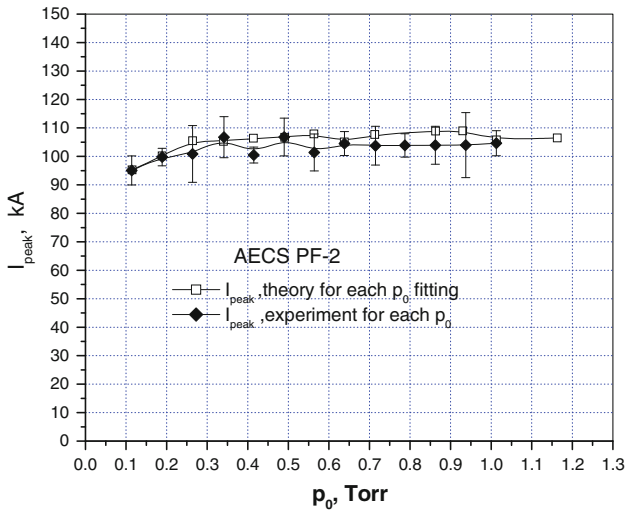

Fig. 6 Comparison of measured and calculated peak current values I_{peak} versus pressure in argon at AECS PF-2

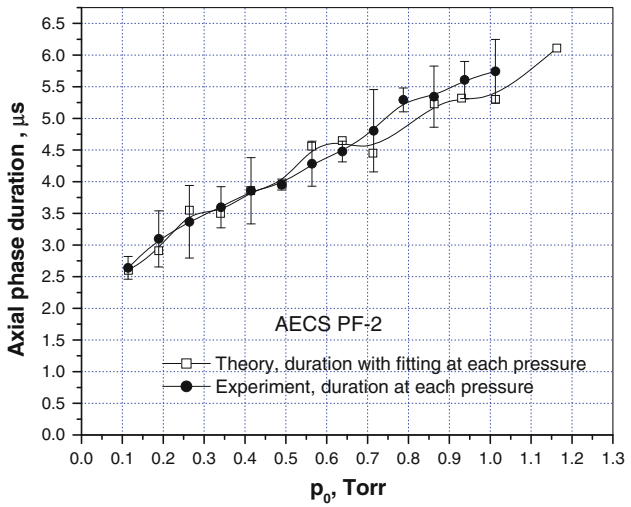

Fig. 7 Comparison of the measured and calculated axial phase duration versus pressure in argon at AECS PF-2

Conclusion

In this work, we have fitted the computed current waveforms to the measured current waveforms using Lee model code RADPF 5.15.d for AECS PF-2 and INTI PF to find the model parameters versus pressure of filling gases (Ar & Ne). For two devices, we obtained a good fit of all features from the start to the end of the axial phase. With the present current measurement set-ups the measured radial phase current dip is too noisy to allow accurate fitting. The results show a value of $f_m = 0.05 \pm 0.01$ ($\pm$ 20%) over the whole range of pressure 0.2–1.2 Torr in Ar; and $f_m = 0.04 \pm 0.01$ ($\pm$ 25%) over 0.7–4.1 Torr in Ne. The value of $f_c = 0.7$ was fitted for all cases. Combining these results with those published for several other small machines, it would appear that, where measured current waveforms are not available for example in designing new machines, a good compromise would be to take a guideline value of $f_m = 0.05$ and $f_c = 0.7$ for both argon and neon.

We have designed another current measurement system based on numerically integrating a dI/dt waveform measured with a Rogowski coil of a few turns. This will allow measurements to be made of the radial phase model parameters.

Acknowledgments The first two authors would like to thank the director general of AEC of Syria, for his encouragement, guidance and permanent support.

References

1. J.W. Mather, Phys. Fluids **8**, 366 (1965)
2. S. Lee, T.Y. Tou, S.P. Moo, M.A. Eissa, A.V. Gholap, K.H. Kwek, S. Mulyodrono, A.J. Smith Suryadi, W. Usada, M. Zakaullah, Am. J. Phys. **56**, 62 (1988)
3. S. Lee, IEEE Trans. Plasma Sci. **19**, 912 (1991)
4. L. Mahe, Soft X-rays from compact plasma focus" Ph D Thesis, School of Science, Nanyang Technoloical University, December 1996, Ch. 5, p. 143
5. S. Heoh, P. Lee, R.S. Rawat, S. Lee, IEEE Trans. Plasma Sci. **37**(7), 1276–1282 (2009)
6. S. Lee, P. Lee, S.H. Saw, R.S. Rawat, Plasma Phys. Control. Fusion **50**, 8 (2008). 065012
7. M. Akel, Sh. Al-Hawat, S.H. Saw, S. Lee, J. Fusion Energ. **29**, 223–231 (2010)
8. S. Lee, S.H. Saw, P. Lee, R.S. Rawat, H. Schmidt, Appl. Phys. Lett. **92**(12) (2008)
9. S. Lee, Theoretical Basis: Plasma focus Model (radiative)—S Lee Model, http://www.plasmafocus.net/IPFS/modelpackage/file/RADPF.htm (October 2010) Or http://intimal.edu.my/school/fas/UFLF/2010
10. S. Lee, Radiative dense plasma focus computation package (2008), RADPF http://www.intimail.edu.myLschoolL fas/UFLF/
11. T.Y. Tou, PhD Thesis, Univ. of Malaya, Malaysia, (1986)
12. S. Al-Hawat, S. Saloum, Contrib. Plasma Phys. **49**(1), 5–14 (2009)
13. S. Lee, Experiments with the ICTP-UM 3.3 kJ Plasma Fusion facility, Spring College on Plasma Physics, International Center For Theoretical Physics (ICTP), Trieste, Italy, May 17–June 11 (1993)